Transport Pathways and Enhancement Mechanisms within Localized and Non-Localized Transport Regions in Skin Treated with Low-Frequency Sonophoresis and Sodium Lauryl Sulfate

Citation: Polat, Baris E., Pedro L. Figueroa, Daniel Blankschtein, and Robert Langer 2011Transport Pathways and Enhancement Mechanisms Within Localized and Non-localized Transport Regions in Skin Treated with Low-frequency Sonophoresis and Sodium Lauryl Sulfate. Journal of Pharmaceutical Sciences 100(2): 512–529.

As Published: http://dx.doi.org/10.1002/jps.22280

Publisher: Wiley Blackwell

Persistent URL: http://hdl.handle.net/1721.1/78862

Version: Author's final manuscript: final author's manuscript post peer review, without publisher's formatting or copy editing

Published in final edited form as:
J Pharm Sci. 2011 February ; 100(2): 512–529. doi:10.1002/jps.22280.

Transport Pathways and Enhancement Mechanisms within Localized and Non-Localized Transport Regions in Skin Treated with Low-Frequency Sonophoresis and Sodium Lauryl Sulfate

Baris E. Polat, **Pedro L. Figueroa**, **Daniel Blankschtein**[*], and **Robert Langer**
Department of Chemical Engineering, Massachusetts Institute of Technology, Cambridge, MA 02139, USA

Abstract

Recent advances in transdermal drug delivery utilizing low-frequency sonophoresis (LFS) and sodium lauryl sulfate (SLS) have revealed that skin permeability enhancement is not homogenous across the skin surface. Instead, highly perturbed skin regions, known as localized transport regions (LTRs), exist. Despite these findings, little research has been conducted to identify intrinsic properties and formation mechanisms of LTRs and the surrounding less-perturbed non-LTRs. By independently analyzing LTR, non-LTR, and total skin samples treated at multiple LFS frequencies, we found that the pore radii (r_{pore}) within non-LTRs are *frequency-independent*, ranging from 18.2 – 18.5 Å, but significantly larger than r_{pore} of native skin samples (13.6 Å). Conversely, r_{pore} within LTRs *increases significantly with decreasing frequency* from 161 Å, to 276 Å, and to ∞ (>300Å) for LFS/SLS-treated skin at 60 kHz, 40 kHz, and 20 kHz, respectively. Our findings suggest that different mechanisms contribute to skin permeability enhancement within each skin region. We propose that the enhancement mechanism within LTRs is the *frequency-dependent process* of cavitation-induced microjet collapse at the skin surface, while the increased r_{pore} values in non-LTRs are likely due to SLS perturbation, with enhanced penetration of SLS into the skin resulting from the *frequency-independent process* of microstreaming.

Keywords

Diffusion; Permeability; Permeation Enhancers; Skin; Surfactants; Transdermal; Transdermal Drug Delivery; Ultrasound

INTRODUCTION

The use of ultrasound to increase skin permeability, referred to as sonophoresis, has generated considerable interest and gained much use over the past few decades.[1] Initial research in the field was conducted at therapeutic frequencies, 1–3 MHz,[2–4] while more recent research efforts have focused on low-frequency sonophoresis (LFS), in the range 20–100 kHz. This shift in frequencies was prompted by the discovery that cavitation is the primary mechanism responsible for skin permeability enhancement.[5–9] The observed frequency dependence of cavitation occurs because of the inverse relationship between the ultrasound frequency and the radii of the cavitation bubbles generated in the coupling medium between the ultrasound horn and the skin.[10–12] As the ultrasound frequency

---

[*] Corresponding author: Professor Daniel Blankschtein, Department of Chemical Engineering, Room 66-444, Massachusetts Institute of Technology, 77 Massachusetts Avenue, Cambridge, MA 02139, USA, Tel: +1 617 253 4594, Fax: +1 617 252 1651, dblank@mit.edu.

decreases, the radii of the cavitation bubbles tend to grow on average, resulting in more forceful collapses when cavitation bubbles approach the surface of the skin. These transient cavitation events near the skin surface have been identified as the primary mechanism of skin permeability enhancement in response to LFS treatment.[5,6,8]

In addition to uncovering the connection between cavitation and skin permeability enhancement, recent research has revealed many additional interesting phenomena. First, it has been demonstrated that when LFS and chemical enhancers, especially surfactants, are applied simultaneously during skin treatment, a synergistic enhancement is observed.[6,13] This synergism can lead to an increase in skin conductivity or permeability by orders-of-magnitude when compared to skin treated separately with LFS or chemical enhancers.[13–15] Second, it has been shown that skin permeability enhancement by LFS and by LFS/SLS at 20 kHz is not homogenous.[15–21] Instead, the LFS treatment generates discrete regions within the skin, referred to as localized transport regions (LTRs), which are orders-of-magnitude more permeable than the surrounding skin regions (non-LTRs) and native skin samples.[14] Furthermore, it has been shown that the non-LTRs also exhibit increased skin permeability, with respect to native skin, when treated with 20 kHz LFS in combination with the surfactant sodium lauryl sulfate (SLS).[14,17,21] Accordingly, it was proposed that two levels of enhancement are present in skin samples that are treated simultaneously with LFS at 20 kHz and a chemical enhancer, such as SLS. The proposed existence of two levels of enhancement on a single skin sample in response to LFS/SLS at 20 kHz suggests that separate mechanisms of enhancement may operate within the LTRs and the non-LTRs, or that an enhancement mechanism that is significant within the LTRs does not play a role within the non-LTRs. This possibility motivates the need for a deeper understanding of the transport pathways within LTRs and non-LTRs. In addition to quantifying the relative extents of skin perturbation by measuring skin permeability and skin resistivity, it is possible to utilize the aqueous porous pathway model[22] and previously published masking techniques[14] to independently probe the effective pore radii in the LTRs and the non-LTRs. In doing so, one may be able to provide deeper insight into the nature of the aqueous transdermal pathways that exist within LTRs and non-LTRs, including the permeability enhancement mechanisms that are most significant in each of these skin regions. Moreover, because acoustic cavitation bubble collapse on the skin surface is a frequency-dependent process,[10–12] with the average cavitation bubble radius increasing with decreasing ultrasound frequency, one would expect that the average pore radii in the skin regions where such collapses occur would also increase with decreasing ultrasound frequency, if this mechanism was present.

It is important to note that a previous study investigated the average pore radius of skin treated with a range of LFS frequencies, in the context of the aqueous porous pathway model.[19] However, because that study did not independently study LTRs and non-LTRs, it is significantly different than the study presented here. First, because the pore radii within LTRs and non-LTRs were not studied separately, no direct conclusions could be reached about the nature of the transport pathways or enhancement mechanisms within LTRs and non-LTRs. Second, the ultrasound intensity used in the previous study was 1.08 W/cm^2, which is significantly lower than the 7.5 W/cm^2 ultrasound intensity used in the experiments reported here. Note that the ultrasound intensity used here is similar to those used in other recent papers discussing LTR formation using LFS/SLS.[14–17,23] Third, the range of skin electrical resistivities investigated here is lower than that of the previous study, indicating that the skin samples considered here are perturbed to a greater extent by the LFS/SLS treatment than those considered in the prior study. In fact, because LTR size is closely related to the extent of skin perturbation, as measured by skin resistivity,[14] it is likely that any LTRs that were formed would be much smaller than those observed in the study reported here. Because the effects of the enhancement mechanisms are expected to be magnified under the ultrasound skin treatment conditions used in this study, relative to those used previously, the combination of a higher ultrasound intensity and a greater extent of skin perturbation by the LFS/SLS treatment utilized here should facilitate gaining insight into the enhancement mechanisms at play within LTRs and non-LTRs, including the effect of the ultrasound frequency on the resulting transdermal pathways in each skin region.

With all of the above in mind, the goals of this paper are four-fold: i) to demonstrate that at the three ultrasound frequencies tested (20 kHz, 40 kHz, and 60 kHz), LTRs form on the surface of the skin and exhibit increased permeability relative to both the non-LTRs and native skin, ii) to demonstrate that at the three frequencies considered here there are two levels of skin permeability enhancement relative to native skin when LFS and SLS are used simultaneously, indicating that the non-LTRs also exhibit increased permeability relative to native skin, iii) to better characterize the transport pathways through LTRs and non-LTRs by independently determining the permeabilities and the effective aqueous pore radii in LTRs, non-LTRs, and total skin samples in the context of the aqueous porous pathway model, and iv) to propose mechanisms of enhancement within LTRs and non-LTRs.

MATERIALS AND METHODS

Chemicals

Phosphate buffer saline (PBS; 0.01 M phosphate, 0.137 M NaCl), calcein, and SLS were obtained from Sigma Chemical Company (St. Louis, MO). The dye allura red (molecular weight = 496 g/mol, water solubility = 225 g/L = 22.5 wt% at 25 °C, log $K_{O/W}$ =−0.550 [24]) was obtained from TCI America (Portland, OR). C_{14}-labeled SLS (specific activity of 55 mCi/mmol) was obtained from American Radiolabeled Chemicals (St. Louis, MO). Soluene-350, a tissue solubilizer, and Hionic-Fluor, a scintillation cocktail, were obtained from Perkin-Elmer (Waltham, MA). All chemicals were used as received.

Skin Preparation

Previously published protocols were utilized for the storage and preparation of skin samples.[22] A brief summary of these protocols follows. This procedure has been approved by the MIT Committee on Animal Care. Skin was harvested from the back and flank of Female Yorkshire pigs within 1 hour of sacrificing the animal. Subcutaneous fat was removed from the skin using a razor blade and then sectioned into one-inch strips prior to storage at −85 °C for up to 6 months. Before use in experiments, the skin was thawed for 1 hour in PBS and then excess hair was trimmed using surgical scissors. The thawed skin was then cut into 25 mm by 25 mm samples. Before mounting of the skin samples into the 15-mm inner diameter diffusion cells (PermeGear, Hellertown, PA), high vacuum grease (Dow Corning, Midland, MI) was applied to the inner flange of the donor and the receiver compartments in order to provide a water-tight seal between the skin and the diffusion cell. For additional mechanical support, a 150-μm opening nylon mesh (Sefar Filtration, Depew, NY) was placed onto the top of the receiver chamber of the diffusion cell. The receiver chamber was then filled with PBS, the skin sample was mounted into the diffusion cell, and the diffusion cell was clamped tightly. The donor chamber was then filled with the appropriate solution for treatment or permeation experiments.

Skin Electrical Resistivity Measurements

The skin electrical resistivity, R, has been shown to be an accurate and instantaneous indicator of the structural state of the skin.[25,26] Previously published methods were followed to measure R[16,23,26] and are summarized next. A signal generator (Hewlett-Packard, model HP 33120A) was used to generate an AC voltage at 100 mV and 10 Hz. The voltage was applied across the skin using two Ag/AgCl electrodes (In Vivo Metrics, Healdsburgh, CA).

The skin electrical current was measured using a multimeter (Fluke Corporation, Model 189) and the skin electrical resistance was calculated using Ohm's Law. The background resistance of the system was accounted for by removing the skin sample from the diffusion cell and measuring the resistance of the system (note that this resistance is a function of the area available for diffusion, therefore the background resistances for the LTRs and the non-LTRs are not necessarily the same as that for the total skin samples). Subsequently, the background resistance was subtracted from the resistance measured for the total system, including the skin. R was then calculated by multiplying the skin electrical resistance by the area of the skin sample. In order to ensure that the skin was intact prior to experimentation, the initial R value of a skin sample was required to be above 50 $\mathrm{kOhm\cdot cm^2}$.[27–29] The electrical current measured, and the resulting resistivity values, were calibrated by testing the electrical equipment with resistors of known resistance.

Determination of Steady-State Calcein Permeabilities through the Skin

Calcein was chosen as a model aqueous permeant because its concentration in aqueous solution can be determined with relative ease using simple spectrophotometric methods, which minimizes sample preparation time and the cost of sample analysis. Calcein has also been used in the past to determine skin permeabilities in the context of the aqueous porous pathway model.[14] The procedures described in the following sub-sections were carried out on LTRs, non-LTRs, and total skin samples, as well as on native skin and skin dermis.

Pre-Treatment of Skin Samples by LFS/SLS—LFS/SLS pre-treatment of skin samples was carried out according to previously published methods, which are summarized next.[14–17,22] Three separate ultrasound systems (Sonics and Materials, Inc., Newtown, CT) were used in this study, each operating at a different frequency: 20 kHz (VCX 500), 40 kHz (VCX 130), and 60 kHz (custom order). The intensity of each horn was calibrated using calorimetry, and the skin treatment with each system was carried out under identical experimental conditions: intensity − 7.5 $\mathrm{W/cm^2}$, duty cycle - 50% (5 s on, 5 s off), tip displacement - 3 mm, and a coupling medium containing 1% (w/v) SLS and 0.025% (w/v) allura red in PBS. Samples were treated with LFS until they reached pre-determined electrical current thresholds of 225, 275, or 335 μA (±10%), which are similar to previously published thresholds used when studying LTR formation.[14,23] These thresholds were chosen in order to: i) create LTRs that are sufficiently large to be quantifiable on a macroscopic scale (at least 5% coverage of LTRs on the skin surface), and ii) study different levels of skin perturbation. After each minute of LFS treatment, the coupling medium was changed in order to minimize thermal effects (maintain the temperature within 10 °C of room temperature), and the electrical current of the skin samples was measured to determine if the target threshold had been reached. Upon completion of the LFS treatment, samples were rinsed thoroughly with PBS, in order to remove all excess SLS from the skin surface, and then the donor solution was replaced with 0.025% (w/v) allura red in PBS for 1 hour. Because of the significantly higher permeability of LTRs, relative to non-LTRs (see Results section), increased uptake of allura red occurs significantly only within LTRs during the additional 1 hour soak, which aids in the subsequent digital imaging of the LTRs.

Digital Imaging and Analysis of LTR Areas—Digital imaging and analysis of LTRs was conducted according to previously published protocols, which are summarized next.[14] After the 1-hour soak in the allura red solution, the skin samples were thoroughly rinsed with PBS and blotted dry. The skin samples were then imaged in triplicate using a digital camera (HP Photosmart R967, 10 Megapixels, auto macro setting) at a distance of approximately 8 inches above the sample. In order to correct for fluctuations in laboratory lighting and infidelity of the charged coupled device, a red-colored strip was included in each image as a standard (VWR, general-purpose laboratory labeling tape, color "red").

Images were then analyzed using the Corel Photo-Paint 11 Software Package (Corel Corporation, Ontario, Canada) according to the method published by Kushner *et al*.[14] Briefly, first the red-colored tape strip in each image was isolated in order to measure the average blue-channel levels for all of the isolated strips. Then, the blue level for each image was shifted using the "Contrast Enhancement" function to the average blue level for all samples. After this standardization, the images were cropped to the size of the skin sample treated by LFS (15 mm by 15 mm image size). Subsequently, the total number of pixels in the image was noted using the "Histogram" function. In order to determine the size of the LTRs, the "Threshold" function was used to tabulate the number of pixels having a blue-channel level below 50. The reasons for the selection of these criteria are discussed further in Kushner *et al*.[14] It is important to note that the blue level threshold used in the current study is different than that used by Kushner *et al*., because we utilized allura red to visualize the LTRs instead of sulforhodamine B (SRB).[14] SRB was not used in the present study because a fluorescent dye was not required. It is then straightforward to calculate the area of the LTRs on the skin surface, A_{LTR}, in terms of the number of LTR pixels, the total number of pixels in the image, and the total area of the image (A_{total} =1.5 cm by 1.5 cm = 2.25 cm^2). Specifically,

$$A_{LTR}=\frac{(\text{LTR Pixels})}{(\text{Total Pixels})}\cdot A_{total} \tag{1}$$

Diffusion Masking Experiments—Diffusion masking is a previously published method[14] that allows one to probe the transport properties of the LTRs and the non-LTRs separately. Use of this method allowed us to test three groups of samples at each ultrasound frequency following pre-treatment with LFS/SLS: total, LTR, and non-LTR samples. Skin samples in the total group were not masked (indicating that the entire skin surface was available for calcein permeation). Skin samples in the LTR group had the non-LTR regions masked in order to leave the LTR regions accessible for permeation of calcein (see Figure 1 for an image of a skin sample showing LTRs and non-LTRs). Similarly, skin samples in the non-LTR group had the LTR regions masked in order to leave the non-LTR regions accessible for permeation of calcein. The masking technique involves applying vacuum grease to either the LTR or the non-LTR regions, respectively. The vacuum grease does not allow diffusion of hydrophilic permeants through the skin regions that are masked with vacuum grease. This method has been validated previously by Kushner *et al.*[14]

Calculating the Steady-State Calcein Permeability through the Skin—Following imaging and masking, all skin samples were remounted into clean, dry diffusion cells. The receiver chamber of each sample was filled with PBS (12 mL) and the donor chamber was filled with 2.5 mL of 0.2% (w/v) calcein in PBS solution. These experiments were conducted at room temperature (25 °C), and the receiver chambers were magnetically stirred at 400 rotations per minute. Samples were allowed sufficient time to reach steady-state (which has previously been established for calcein through porcine skin[14]), and then were sampled at two-hour intervals between 18 – 26 hours after initiation of the experiments. For each sample, a 1 mL aliquot was withdrawn from the receiver chamber and immediately replaced with an equal volume of PBS. In addition, at each time interval, a 20 μL aliquot was withdrawn from the donor chamber and diluted to 2 mL (in order for the absorbance to be in the linear regime for calcein). The concentration of calcein in each aliquot was determined using a UV/VIS spectrophotometer (Beckman Coulter DU 800) to measure absorbance at λ = 494 nm and, subsequently, was converted to units of % (w/v) using a standard curve generated from known concentrations of calcein.

Finally, the permeability of calcein through the skin, P, was calculated at steady-state, infinite sink conditions using the following equation:

$$P=\frac{V}{AC_d}\left(\frac{\Delta C}{\Delta t}\right) \tag{2}$$

where A is the area of skin available for permeation (which can vary with LTR area for the masked samples, with $A = 1.77\ \text{cm}^2$ for the total skin samples), V is the volume of PBS in the receiver chamber, C_d is the average calcein concentration in the donor chamber over the sampling period, and ($\Delta C/\Delta t$) is the rate of change of calcein concentration in the receiver chamber (where replacement of the sampled aliquots by PBS is taken into account).

As previously noted, three main skin sample groups were studied: total samples, LTR samples, and non-LTR samples. In addition, passive samples were also tested, which involved no LFS/SLS pre-treatment, in order to compare the permeabilities of LTRs and non-LTRs to that of native skin. Note that in the non-LTR and passive sample groups, it was necessary to account for the background absorption of lipids in the receiver chamber in the spectrophotometric analysis. It is well established that many epidermal and dermal components have broad range absorption in the visible light range,[30–34] which justifies the need for this correction when the absorption of calcein is of similar, or of lower, magnitude than the absorption of the skin components in solution at the wavelength of interest. This procedure is described in Appendix A. Because there is a higher concentration of calcein present in the receiver chambers of LTR samples, background absorption was found to be insignificant within these samples and, therefore, there was no need to implement the procedure described in Appendix A.

Calcein Permeability through the Skin Dermis—The final group of samples consisted of skin that was first dermatomed (Zimmer Electric Dermatome, Model 8821, Dover, OH) at a depth of 300 μm to completely remove the entirety of the epidermis from the dermis. The epidermis was then discarded, and the calcein permeability and skin electrical resistivity of the dermis were measured. Note that the calcein permeability and skin electrical resistivity of the dermis are necessary in order to find the effective aqueous pore radius of the dermis in the context of the aqueous porous pathway model (see "Theory" section).[22]

Experiments with C_{14}-Labeled SLS

In order to quantify the amount of SLS partitioning into the LTRs, the non-LTRs, and the passive samples, the skin was pre-treated as described in the section "Pre-Treatment of Skin Samples by LFS/SLS", but the coupling medium also contained 0.5 μCi/mL C_{14}-labeled SLS, in addition to the 1% (w/v) SLS, and 0.025% (w/v) allura red in PBS. Skin samples were treated with 20 kHz ultrasound for a total on time of 10 minutes (20 minutes at 50% duty cycle), resulting in skin samples with an average current of 330 μA (within the range of currents tested in the experiments used when calculating calcein permeabilities). Following treatment, skin samples were rinsed with PBS, blotted dry with lab tissue, and then LTRs (that were dyed red, see Figure 1) and non-LTRs (the undyed skin regions, see Figure 1) were sampled using a circular cutting tool with an area of 7.9 mm^2. On each skin sample, it was typically possible to sample 2–3 LTR samples and 4–7 non-LTR samples (since the non-LTRs occupy larger areas on the skin). The skin samples were then solubilized using Soluene-350 (1.5 mL), and the amount of SLS was quantified using a Tri-Carb Liquid Scintillation Counter (Perkin-Elmer), utilizing the scintillation cocktail Hionic-Fluor (5 mL). This process was repeated for ten skin samples. Passive samples were contacted with the

C_{14}-labeled SLS-containing coupling medium for 20 minutes. For passive samples, the entire skin sample that contacted the solution (with area of 1.77 cm^2) was used to quantify the amount of SLS in the skin. For the case of the larger passive samples, 5 mL of Soluene-350 and 15 mL of Hionic-Fluor were utilized in the analysis of each sample. This process was repeated for 20 skin samples. For all samples, the concentration of SLS in the skin was normalized by the surface area of that sample.

In addition, to further test the mechanism of SLS penetration into non-LTRs, experiments were conducted to quantify the penetration of SLS into the skin for two additional cases: i) with increased temperature of the donor solution, and ii) with vigorous stirring in the donor compartment of the diffusion cell. During ultrasound application, the temperature of the donor solution increases linearly from room temperature (25 °C) by no more than 10 °C during a two-minute treatment (with 50% duty cycle and 1-minute ultrasound ON time). Therefore, to quantify the effect of just the temperature increase on SLS penetration into the skin, an identical donor solution to that described above was initially heated to 37 °C (body temperature and approximately 10 °C higher than room temperature) and was contacted with the skin in two-minute increments (the same time interval corresponding to the ultrasound experiments). The solution was replaced 10 times, with the 37 °C donor solution, for a total contact time of 20 minutes. To test the effect of decreasing the concentration boundary layer above the skin, an experimental setup was designed to allow for rapid stirring of the donor solution above the skin. Samples were prepared by: i) placing a 12.5 mm stir bar (VWR) in the donor compartment (having a diameter of 15 mm), ii) filling the donor compartment with ~1.5 mL of C_{14}-labeled SLS-containing coupling medium, and iii) capping the diffusion cell with a plastic stopper (Chemglass, Vineland, NJ, part# CG-3021-01). Once the samples were capped, the distance between the skin surface and the bottom of the stopper was 5 mm. The diffusion cells were placed underneath a ¼” thick acrylic platform (fabricated in-house) with a magnetic stir plate inverted on top of it (Corning, Lowell, MA, model PC-410). Once the samples were placed under the magnetic stir plate, and the height of the platform was adjusted so that it was resting on top of the diffusion cell, the magnetic stir bar was attracted to the stir plate and therefore rested at the bottom of the plastic stopper (5 mm above the skin surface). It was necessary that the stir bar not contact the skin during mixing, because if the stir bar had rested on the skin surface, it could cause mechanical abrasion of the skin due to friction. The stir plate was then set to its maximum speed, a setting of “10”, and the experiment was allowed to proceed for 20 minutes. Although the LFS/SLS experiments have an LFS ON time of 10 minutes (50% duty cycle), we observed that fluid flow persisted in the donor compartment of the diffusion cell during the LFS OFF time (that is, fluid flow did not cease immediately after LFS was turned off). Accordingly, to better reproduce the environment above non-LTRs in the LFS/SLS experiments, the vigorously-stirred experiments were conducted for 20 minutes (the full contact time of the SLS donor solution with the skin during the LFS/SLS treatment). Both sets of samples were prepared, and the amount of SLS quantified, in the same manner as described earlier in this section for the passive samples contacted with C_{14}-labeled SLS.

THEORY

Calculating the Effective Aqueous Pore Radius of the Skin

In order to calculate the effective aqueous pore radius (r_{pore}) of the skin samples tested, we utilized the aqueous porous pathway model.[22] The main assumption of this model is that aqueous permeants (in this case, calcein) traverse the skin along the same paths as the current carrying ions of the electrolyte solution that the skin is immersed in (for PBS, the dominant ions are Na^+ and Cl^-). This model utilizes hindered transport theory[35] in order to quantify the steric hindrance exerted by the finite-size skin pores on the flux of the aqueous permeant and the current carrying ions through the skin. The hindrance factors corresponding to both species are related solely to the radius of each permeant and r_{pore}. Therefore, by equating the diffusion of the aqueous permeant, which is related to P, and of the current carrying ions, which is related to R, one can determine r_{pore}.

The relation between permeability, P, and skin electrical resistivity, R, in the context of the aqueous porous pathway model, is given by:[22]

$$\log P = \log C - \log R \tag{3}$$

where C is defined as follows:

$$C = \frac{kT}{2z^2 F c_{ion} e_0} \cdot \frac{D_p^{\infty} H(\lambda_p)}{D_{ion}^{\infty} H(\lambda_{ion})} \tag{4}$$

where z is the electrolyte valence, F is Faraday's constant, c_{ion} is the electrolyte molar concentration, e_0 is the electronic charge, k is the Boltzmann constant, T is the absolute temperature, D_i^{∞} is the infinite-dilution diffusion coefficient of solute i, $H(\lambda_i)$ is the hindrance factor for solute i, and λ_i is defined as the ratio of the radius of solute i, r_i, to the radius of the aqueous skin pores, r_{pore}.[14] Although previous work has utilized older expressions for the hindrance factor, $H(\lambda)$,[14,19,22,23,26,36,37] the most advanced expression for $H(\lambda)$, which has been used recently in the context of the aqueous porous pathway model[38] and is valid for $\lambda_i \leq 0.95$, is given by:[35]

$$H(\lambda_i) = 1 + \frac{9}{8}\lambda_i \ln\lambda_i - 1.56034\lambda_i + 0.528155\lambda_i^2 + 1.91521\lambda_i^3 - 2.81903\lambda_i^4 + 0.270788\lambda_i^5 + 1.10115\lambda_i^6 - 0.435933\lambda_i^7 \tag{5}$$

It is important to note that the only variable in Eq. (4) that depends on the intrinsic properties of the skin is r_{pore}. All the other variables are either constants or are properties of the permeants used. Therefore, once an experimental C value is determined using Eq. (3), r_{pore} can be determined by iteratively solving Eq. (4) until C converges.

It is important to stress that, for any given aqueous permeant used (with given hydrodynamic radius, which is 8 Å for calcein[39]), only a certain range of r_{pore} values can be probed in the context of the aqueous porous pathway model. In fact, for any permeant, there will be an upper bound on the r_{pore} values that can be determined depending on the hydrodynamic radius of the permeant. This is due to the fact that, as the pores become increasingly large, the extent of hindrance exerted by the pores on the diffusing permeant becomes increasingly small as the hindrance factor approaches unity (recall that hindrance factors range from 0 to 1, where a hindrance factor of 1 corresponds to no hindrance and a hindrance factor of 0 corresponds to infinite hindrance). Beyond a certain r_{pore} value, the hindrance exerted by the pores on the permeant becomes statistically indistinguishable from the diffusion of the permeant at infinite dilution, which corresponds to the upper bound of r_{pore} that can be probed with that permeant. This infinite-dilution limit (also known as an infinite-pore limit) will be attained at lower r_{pore} values for smaller permeants and will be higher for larger permeants. This limit can be estimated in one of two ways: i) Assuming that, beyond a certain r_{pore} value, the hindrance factor calculated for calcein cannot be differentiated from a hindrance factor of unity. In past publications, the level of uncertainty in the hindrance factor was chosen to be 10%, and the pore radius corresponding to $H(\lambda) = 0.9$ was chosen as the upper bound for a given permeant,[22] or ii) Assuming that the pores within the hydrophilic dermis are infinite, and then using the pore radius calculated for the dermis in the context of the aqueous porous pathway model as the upper limit on r_{pore}. We tested both methods, and they both yielded a similar upper limit of r_{pore} for calcein, approximately 300 Å.

In order to apply the aqueous porous pathway model to our data, a linear regression was fit to each set of log P versus log R values. For the model to be applicable, we required that the 95% confidence interval of the slope corresponding to every given data set includes the theoretical value of −1 (see Eq. (3)). Once this test was carried out, and we confirmed that the data was described by the aqueous porous pathway model, a C value was determined using Eq. (3) for each data point tested. Subsequently, all of the individual C values within each data set were averaged to yield the C value for that data set. This C value was then used to calculate r_{pore} in the manner described above. Therefore: i) the reported r_{pore} value for a given data set is calculated from the mean value of C for that data set, and ii) the 95% confidence interval reported for r_{pore} is calculated from the 95% confidence interval for C for each data set. In general, all the statistical analyses reported in this study involve two-sampled t-tests, at 95% confidence, unless noted otherwise.

Calculating the Skin Porosity-to-Tortuosity Ratio

In order to gain deeper insight into the transdermal pathways present within each skin region, it is possible to again implement the aqueous porous pathway theory to calculate the ratio between the skin porosity, ε, and the skin tortuosity, τ, using the following expression:[22]

$$\left(\frac{\varepsilon}{\tau}\right)_i=\frac{1}{\left(\frac{R_i}{\Delta x}\right)\sigma_{sol}H(\lambda_{ion,i})} \tag{6}$$

where the subscript i denotes a given skin sample, σ_{sol} is the electrical conductivity of PBS (0.012 Ω^{-1}cm^{-1}),[22] $H(\lambda_{ion,\,i})$ is the hindrance factor for an ion calculated using Eq. (5), R_i is the skin electrical resistivity, and Δx is the thickness of the skin layer that provides the primary barrier to transport. For the non-LTRs and passive skin samples, Δx can adequately be defined as the thickness of the stratum corneum, or 13.1 μm.[40] Selecting an appropriate Δx value for LTRs will be further discussed in the Results section.

RESULTS AND DISCUSSION

Dependence of the LTR, non-LTR, and Total Calcein Permeabilities on Electrical Current Treatment Threshold and Ultrasound Frequency

Figure 2 shows the calcein permeability data for each of the three groups of samples tested (total, LTR, and non-LTR) at the three ultrasound frequencies considered (A - 20 kHz, B - 40 kHz, and C - 60 kHz). In addition, the passive group is included in these figures for comparison to the calcein permeability of native skin. As illustrated in Figure 2, at all three frequencies, the permeability of calcein through the LTRs is much greater than those through all the other skin regions. Additionally, we note that the permeability within LTRs is of similar magnitude to the permeability within dermis samples ($P = 1.8\cdot10^{-2}$ cmhr, calculated as described in the Materials and Methods section “Calcein Permeability through the Skin Dermis”), suggesting that much of the barrier properties within the epidermis of these regions has been overcome. These findings are consistent with previous results at 20 kHz.[15] Moreover, at the three frequencies studied, the non-LTRs are also more permeable than the native skin samples, which is consistent with earlier findings at 20 kHz.[14,17,21] As expected, the calcein permeabilities of the total skin samples fall between those of the LTRs and the non-LTRs at each of the three frequencies studied, because these samples contain both types of skin regions.

Figure 2 also shows that for the total skin samples, at each of the three frequencies studied, the calcein permeability increases linearly as a function of the skin electrical current threshold (r^2 =0.94–0.98). In spite of the observed upward linear trend in calcein permeability for the total skin samples, the permeabilities within the LTRs and the non-LTRs exhibit no dependence on the electrical current threshold based on statistical analysis of the data at the three frequencies studied. This indicates that, as the electrical current threshold increases, the permeability of the skin increases due to an increase in the area of the LTRs present on the skin. This is clearly seen in Table 1, where the LTR area increases with increasing skin electrical current threshold for the three frequencies studied. Additionally, by comparing the calcein permeability of the total skin samples, at each current threshold, as a function of ultrasound frequency, we see that the total calcein permeabilities generally decrease with increasing ultrasound frequency (Figures 2A–C). This suggests that the calcein permeation through the skin in the total skin samples is more hindered with increasing frequency. This result will be discussed more thoroughly in the context of the aqueous porous pathway model in the following sections.

Finally, by comparing the calcein permeability data in each skin region tested, one can quantify the relative perturbation in these regions by calculating a permeability enhancement ratio ($P/P_{passive}$). In general, LTR samples are over four orders-of-magnitude more permeable than native skin, and well over two orders-of-magnitude more permeable than non-LTR samples. In addition, non-LTRs are over thirty-fold more permeable than native skin. This again confirms the earlier finding that two levels of enhancement are observed when treating skin simultaneously with LFS at 20 kHz and a chemical enhancer, such as SLS.[14,17,21] In the following sections, we will discuss in more detail possible causes leading to the observed two levels of enhancement in the context of the effective aqueous skin pore radii in the different skin regions.

Determining Effective Aqueous Pore Radii in LTRs, non-LTRs, and Total Skin Samples as a Function of Ultrasound Frequency

Figure 3 shows the log P vs. log R plot used to analyze the 40 kHz LTR data in the context of the aqueous porous pathway model. In order for the model to be applicable, it is first necessary to check whether each data set's linear regression has a slope that is not statistically different (95% confidence) from the theoretical value of −1 (see "Theory" section). The results of this analysis are reported in Table 2, which shows that all the data sets have slopes that are within valid limits for the aqueous porous pathway model to be applicable. The r^2 values for all the data sets, except for the passive skin samples, are also within the expected range reported in previously published data.[22] Note that the low r^2 value exhibited by the passive skin sample set can be rationalized as follows. The skin resistivity values for the passive skin samples are grouped very closely to each other, given the resistivity of native skin and the fact that we require that the skin samples used possess sufficiently high initial resistivity to ensure that they are not damaged. Therefore, any scatter in the permeability data due to natural variations in the native skin has a very large effect on the r^2 value for this data set. Unlike in the LTR, non-LTR, and total skin samples, we are not treating samples in a controlled manner to a pre-determined current threshold. Therefore, the data is very susceptible to natural variations in the skin barrier, which can be significant from sample-to-sample and especially between animals. Nevertheless, the passive skin samples provide a good baseline for comparison to the values obtained in the case of the LFS/SLS-treated skin samples and, therefore, have been included in Table 2.

The r_{pore} values corresponding to the different skin regions studied, calculated in the context of the aqueous porous pathway model, are reported in Table 3. The total skin samples clearly exhibit a decrease in r_{pore} with increasing ultrasound frequency. Utilizing a two-sample t-test at 95% confidence, we determined that, for the total skin samples, the difference between r_{pore} calculated at 20 kHz (105 Å) and 40 kHz (73.9 Å), and at 40 kHz and 60 kHz (50.7 Å) are statistically significantly different. We also note that a previous study by our group investigated the effect of different permeants on skin pore radii with 20 kHz LFS/SLS under nearly identical treatment conditions utilizing human skin.[23] In this study, the reported pore radii are very similar to the r_{pore} value reported here for calcein (molecular weight = 622.6 g/mol, r_{pore} = 105 Å) at 20 kHz, for two other hydrophilic permeants with molecular weights greater than 500 g/mol (for raffinose, r_{pore} = 98 Å and for inulin, r_{pore} = 95 Å). Another recent study also found that the average pore radius for porcine skin treated with 20 kHz LFS/SLS, under identical treatment conditions to those utilized in this manuscript, is 113 Å, utilizing sucrose as a model hydrophilic permeant.[38] This confirms that the data reported here at 20 kHz is consistent with the 20 kHz data reported previously.

In order to explain the observed change in the r_{pore} values with ultrasound frequency in the total skin samples, it is revealing to examine the frequency dependence of the r_{pore} values in the LTRs and non-LTRs. Table 3 clearly shows that within the non-LTRs, r_{pore} is independent of the applied ultrasound frequency. Specifically, the r_{pore} values in the non-LTRs remain nearly constant, ranging from 18.2 – 18.5 Å for the three ultrasound frequencies studied, with no statistically significant difference between the three samples. However, these r_{pore} values are statistically significantly larger than the r_{pore} value observed in the passive skin samples (r_{pore} = 13.6 Å). We note that the r_{pore} value for native skin that we have determined is consistent with r_{pore} values for native porcine skin reported in the literature (11 – 28 Å).[41–43] Although the calculated r_{pore} values for both the non-LTRs and native skin samples fall within the range of r_{pore} values reported in the literature for native skin, it is important to stress that, with very high statistical certainty ($P<0.00001$), the calculated r_{pore} values are in fact statistically significantly different in the non-LTR and native skin samples. Accordingly, although there is a statistically significant enhancement in r_{pore} within the non-LTRs relative to the native skin samples, the r_{pore} enhancement observed within the non-LTRs *is not frequency dependent*. On the other hand, within the LTRs, Table 3 clearly shows that there is a frequency dependence of r_{pore}. Similar to what is observed for the total skin samples, as the ultrasound frequency decreases, the r_{pore} values increase from 161 Å at 60 kHz, to 276 Å at 40 kHz, and then to ∞ (>300 Å, the upper-bound for r_{pore} values that can be probed with calcein) at 20 kHz. Because of the observed frequency-independence of r_{pore} in the non-LTRs discussed above, the LTR findings suggests that the observed *increase in the* r_{pore} *values with decreasing ultrasound frequency* in the total skin samples is due primarily to the increase in the r_{pore} values within the LTRs. This result reflects the fact that the total skin samples consist of both LTRs and non-LTRs, with the majority of permeant transport occurring through the LTRs. As a result, the total skin samples exhibit a similar trend in r_{pore} with ultrasound frequency as do the LTRs. However, because the LTRs represent only a small fraction of the surface coverage of the total skin samples (see Table 1), the average r_{pore} values for the total skin samples are significantly lower than those for the LTRs (see Table 3).

Mechanisms of Enhancement in the Non-LTRs of Skin Treated with LFS/SLS

Many mechanisms have been proposed and tested to establish if they play a significant role in skin permeability enhancement with LFS. These include: i) acoustic cavitation in the coupling medium above the skin (stable and transient),[5,6,8,9,44] ii) thermal effects,[9,44] and iii) convection (microstreaming and resulting boundary-layer reduction).[9,44] Of these, only transient cavitation has been consistently identified as the primary mechanism of skin permeability enhancement in LFS, especially transient cavitation events near the surface of the skin.[5,8] These transient cavitation events near the skin surface can perturb the skin either by: i) collapsing as a liquid microjet at the skin surface (either by impacting the skin or impinging into the skin), or ii) spherical collapse near the skin surface (although it has been suggested that spherical collapse close to a membrane may not be a physically achievable process because the interaction between the membrane and the cavitation bubble will likely cause non-linear, or non-spherical, oscillations).[5,45] Note that cavitation *within* the skin has been conclusively shown not to be a significant contributor to skin permeability enhancement when utilizing LFS, but can contribute at higher frequencies.[9] However, in nearly all the mechanistic LFS studies cited, SLS was not utilized in the skin treatment regimen. The absence of SLS is significant, because it has been shown at 20 kHz,[17] and confirmed in this paper at 20 kHz, 40 kHz, and 60 kHz, that two levels of enhancement are present only when a chemical enhancer, such as SLS, is present in the coupling medium during the LFS treatment. Furthermore, none of the mechanistic studies cited above have independently considered LTRs and non-LTRs. In fact, many of these studies were carried out before the existence of LTRs was discovered, including demonstrating that they are regions of high permeability.[14] For these reasons, it is possible that a mechanism that may contribute to non-LTR permeabilization during the LFS/SLS treatment may have been overlooked in earlier studies. With the above in mind, we next examine the previously proposed mechanisms, in the context of our findings, to ascertain if they play a role in permeability and pore radius enhancement within non-LTRs.

It is well established that acoustic cavitation is a frequency-dependent process.[9,10] Accordingly, it is unlikely that cavitation plays a major role in the observed enhancements within the non-LTRs, because we have found that the r_{pore} values in the non-LTRs are frequency-independent (see Table 3). This only leaves heating of the coupling medium and microstreaming as potential mechanisms of enhancement in the non-LTRs. Because our experiments involve a pre-treatment of the skin with LFS and SLS, the only role that heating or microstreaming could play in permeability enhancement in the non-LTRs is to increase the flux of SLS into the skin (note that calcein is not present during the LFS/SLS skin treatment). This is because both heating of the coupling medium and microstreaming are not present in the donor solution post-treatment, and there is no SLS present in the donor solution during the steady-state calcein experiments. Furthermore, it has been shown that ultrasound-induced microstreaming can produce significant agitation of aqueous systems, leading to a decrease in the boundary layer above a membrane to an extent that the boundary layer is insignificant when compared to the boundary layer under passive conditions.[44] In addition, heating is also known to increase permeant diffusion coefficients, and it is therefore possible for this mechanism to increase the flux of SLS into the skin. This leads us to propose that SLS is present in elevated amounts within non-LTRs compared to native skin samples, but in far less amounts than in the highly-perturbed LTRs, due to a mechanism such as microstreaming or heating that is not as significant as cavitation. This proposal is consistent with previous findings, because it has been shown that LFS/SLS treatment of skin increases the penetration of SLS into total skin samples,[14,16] although these studies made no distinction between penetration of SLS into LTRs and non-LTRs.

In order to test the hypothesis that there is increased uptake of SLS in the LTRs and non-LTRs compared to the native skin samples, experiments were conducted (see Methods section, “Experiments with C_{14} Labeled SLS”) to quantify the amount of SLS in LTRs, non-LTRs, and passive skin samples. Additionally, two groups of samples were tested to isolate the effects of vigorous stirring and heating in the donor solution during treatment. Figure 4 shows a comparison of the penetration of SLS into the non-LTRs with those of the vigorously stirred, the heated, and the passive samples (note that the amount of SLS penetrating into the LTRs was not included in Figure 4, in order to more clearly compare the mechanisms associated with SLS penetration into the non-LTRs). It was found that the average amount of SLS in the non-LTRs, per unit area of skin, is $2.51{\cdot}10^{-6}$ mmol/mm^2, which is nearly 2 times greater than that in the native skin samples ($1.40{\cdot}10^{-6}$ mmol/mm^2). In addition, the average amount of SLS in the LTRs ($1.52{\cdot}10^{-5}$ mmol/mm^2), was found to be 11-fold greater than that in the native skin samples. This strongly confirms our hypothesis that SLS is present in increased levels in the non-LTRs compared to the native skin samples, but in far smaller amounts than in the highly-perturbed LTRs. Furthermore, it was found that the SLS concentration in the skin for the vigorously-stirred samples ($2.49{\cdot}10^{-6}$ mmol/mm^2) is statistically similar to that of the non-LTR samples (see 95% confidence intervals in Figure 4). However, the samples whose donor solutions were heated to 37°C showed no significant increase in SLS skin concentration ($1.62{\cdot}10^{-6}$ mmol/mm^2) over the passive samples (see 95% confidence intervals in Figure 4). Therefore, these findings suggest that the dominant mechanism of SLS penetration into the non-LTRs is, in fact, microstreaming-induced reduction of the boundary layer above these skin regions.

Additionally, it is well-established that the effect of SLS perturbation on skin can increase r_{pore} values. Ghosh et al. demonstrated that native skin soaked in PBS has an average pore radius of 20±3 Å, while skin contacted with an SLS solution for five hours has an average pore radius of 33±5 Å.[41] This confirms that it is possible for r_{pore} to increase solely due to the exposure of the skin to SLS. Therefore, we propose that the observed increase in the r_{pore} values in the non-LTRs, and the resulting increase in calcein permeabilities, compared to native skin, is due mainly to the ultrasound-frequency independent process of SLS acting on these skin regions (note that the variability in native skin pore radius distribution may also play a role), where increased penetration of SLS in the non-LTRs is the result of a non-frequency-specific process such as microstreaming (and resulting boundary-layer reduction).

Furthermore, it is important to explain the origin of the observed >30-fold increase in calcein permeability within the non-LTRs, relative to the passive calcein permeability. For this purpose, we model the permeability of calcein through skin as follows:[40]

$$P_{calcein,i}=\frac{H(\lambda_{calcein})_i D^{\infty}_{calcein}}{\Delta x}\cdot\left(\frac{\varepsilon}{\tau}\right)_i \qquad (7)$$

where $P_{calcein,\,i}$ is the calcein permeability through skin sample i, ε_i is the skin porosity of sample i, τ_i is the skin tortuosity of sample i, and all the other variables were defined previously.

Using Eq. (7) to calculate the permeability of calcein through the non-LTR samples, relative to the passive permeability of calcein, and assuming that, in both the non-LTR and passive skin samples, the stratum corneum is the primary barrier to transport (Δx is constant), one obtains:

$$\frac{P_{calcein,non-LTR}}{P_{calcein,passive}}=\frac{H(\lambda_{calcein})_{non-LTR}}{H(\lambda_{calcein})_{passive}}\cdot\left[\left(\frac{\varepsilon}{\tau}\right)_{non-LTR}\Big/\left(\frac{\varepsilon}{\tau}\right)_{passive}\right] \qquad (8)$$

Equation (8) clearly shows that the calcein permeability in the non-LTRs can increase relative to the passive calcein permeability due to: i) a decrease in calcein hindrance (due to an increase in the radii of the skin pores), and ii) an increase in ε/τ. Both of these quantities can be calculated utilizing Eqs. (5) and (8). Note that one can also use Eq. (6), in place of

Eq. (8), to obtain very similar results when calculating the ratio of ε/τ in the non-LTRs and passive skin samples. However, Eq. (8) was used for simplicity. First, we find that, over all the non-LTR samples (recall that there is no frequency dependence within non-LTRs), $\frac{H(\lambda_{calcein})_{non-LTR}}{H(\lambda_{calcein})_{passive}}=\frac{0.081}{0.020}=4.1$. This suggests that the ~35% increase in pore radius observed within non-LTRs, compared to native skin, causes about a 4-fold decrease in calcein hindrance through the skin pores. Next, using Eq. (8), we find that $\left(\frac{\varepsilon}{\tau}\right)_{non-LTR}/\left(\frac{\varepsilon}{\tau}\right)_{passive}=\frac{P_{calcein,non-LTR}}{P_{calcein,passive}}\cdot\left(\frac{H(\lambda_{calcein})_{non-LTR}}{H(\lambda_{calcein})_{passive}}\right)^{-1}=36\cdot(4.1)^{-1}=8.8$. It is important to note that the increase in pore radius that we have calculated for the non-LTRs is embedded within ε/τ, since ε is defined as the area of pores on the skin divided by the total skin area. Therefore, since we have found an approximately 35% increase in pore radius between the non-LTR samples and native skin (18.4 Å and 13.6 Å, respectively), the increase in pore radius can only account for about a 2-fold ($a_{pore}\sim r_{pore}^2$) increase in ε/τ. However, we have just shown that ε/τ increases nearly 9-fold between the non-LTRs and the native skin samples. It therefore follows that the remaining ~4.5-fold increase in ε/τ must be due to either the creation of new pores or to a decrease in τ. Furthermore, using the theoretical derivation found in Kushner *et al.*,[23] the following equation can be used to calculate the ratio between $\tau_{non-LTR}/\tau_{passive}$:

$$\tau=\frac{\left(6t_{lag}D_p^{\infty}H(\lambda_p)\right)^{1/2}}{\Delta x} \tag{9}$$

where t_{lag} is the lag time to reach steady-state diffusion and the remaining variables were defined previously.

Using Eq. (9) for the non-LTR and passive skin samples, with $\Delta x_{non-LTR}=\Delta x_{passive}$, we obtain the following result:

$$\frac{\tau_{non-LTR}}{\tau_{passive}}=\left(\frac{t_{lag,non-LTR}}{t_{lag,passive}}\cdot\frac{H(\lambda_p)_{non-LTR}}{H(\lambda_p)_{passive}}\right)^{1/2} \tag{10}$$

Then, substituting into Eq. (10), noting that t_{lag} is simply the x-intercept on a plot of P vs. time, one finds that $\frac{\tau_{non-LTR}}{\tau_{passive}}=\left(\frac{t_{lag,non-LTR}}{t_{lag,passive}}\cdot\frac{H(\lambda_p)_{non-LTR}}{H(\lambda_p)_{passive}}\right)^{1/2}=\left(\frac{3.1\,\mathrm{hr}}{14.2\,\mathrm{hr}}\cdot\frac{0.081}{0.020}\right)^{1/2}=0.94$. This result implies that the tortuosity has decreased only slightly in the non-LTRs relative to the passive skin samples. Therefore, the majority of the remaining 4.5-fold decrease in ε/τ must be due to increases in porosity due to new pore creation. Nevertheless, it is important to recognize that it is quite possible that SLS acting on the skin can, by itself, cause a change in ε/τ. Indeed, it is well established that surfactants are potent transport enhancers, due to their ability to solubilize/extract lipids and denature corneocytes (keratin fibers).[46] In fact, in the same study in which Ghosh *et al.* investigated the increase in pore radius of skin treated passively with SLS,[41] compared to PBS controls, these authors found that the ε/τ ratio increased by nearly an order-of-magnitude within samples treated with SLS compared to PBS controls, which is consistent with our findings in this study. One can certainly justify the potential of SLS to create new pores on the skin (an increase ε) via the denaturation of corneocytes, which is the most likely explanation for the observed increase in ε/τ based on our findings above. However, more importantly, the analysis presented above confirms that the combined increases in H ($\lambda_{calcein}$) and ε/τ can explain the observed >30-fold (4.1×8.8 = 36) increase in calcein permeability within the non-LTRs relative to native skin.

Mechanisms of Enhancement in the LTRs of Skin Treated with LFS/SLS

Turning our attention next to the observed trend in pore radii in the LTRs, as well as to the related observed trend in the total skin samples, we have found that there is a strong dependence of r_{pore} on the ultrasound frequency (see Table 3). This immediately suggests that cavitation is the primary mechanism of enhancement in the LTRs.[10,12,47] It is also worth stressing that several published papers have reported that transient cavitation events near the surface of the skin are the primary mechanism of overall skin permeability enhancement with LFS.[5,6,8,9,44] One study in particular concluded that cavitation, specifically in the vicinity of the skin, scales directly with overall calcein permeability through rat skin.[48] Accordingly, since we have already concluded that cavitation is not a mechanism of enhancement in the non-LTRs, it follows that this mechanism must be the primary enhancement mechanism in the LTRs.

Further examination of the LTR data in Table 3 shows that the same inverse relationship between the cavitation bubble resonant radius and ultrasound frequency applies to the variation of r_{pore} with ultrasound frequency.[10–12] More specifically, it is well-established that the relationship between the ultrasound frequency (f) and the resonant bubble radius (r_{res}) satisfies the following relationship:[12]

$$r_{res} \cdot f = C_{sol} \tag{11}$$

where C_{sol} is a constant that depends on the properties of the solution in which cavitation is taking place.

Then, by proposing that cavitation microjet collapse onto the surface of the skin is the primary mechanism of skin perturbation and, therefore, that r_{pore} and r_{res} are related directly, we can verify whether the r_{pore} values determined within the LTRs are consistent with the expected variation between the cavitation bubble radius and the ultrasound frequency. Using the same expression given in Eq. (11) to relate r_{pore} and f for the 40 kHz and 60 kHz LTR data, we verify that $C_{sol,\,pore} = r_{res,40kHz} \cdot 40kHz = r_{res,60kHz} \cdot 60kHz$ (to less than 15% error), and we obtain an average $C_{sol,\,pore}$ value equal to $10.3 \cdot 10^3$ kHz · Å. Using this $C_{sol,\,pore}$ value to calculate the expected r_{pore} value at 20 kHz, we obtain a value of 520 Å, which is greater than the infinite-pore limit that we calculated for calcein (r_{pore} >300 Å) and consistent with our data.

Similar to the non-LTR case, it is necessary to explain the origin of the observed increase in calcein permeability within the LTRs (greater than 4 orders-of-magnitude), relative to the passive calcein permeability. However, in the LTR case, because of the decreased barrier properties of the stratum corneum, selecting a suitable value for Δx is more problematic. Fortunately, however, Eq. (6) shows that $\varepsilon/\tau \sim \Delta x$, while Eq. (7) shows that $P \sim (\Delta x)^{-1}$. As a result, the dependence of permeability on Δx cancels out in Eq. (7). For simplicity, in the following analysis we assume that, as is the case for non-LTRs and native skin, Δx is equal to the thickness of the stratum corneum (as has been assumed in previous studies of LTRs[14]). Using Eq. (7) for the LTRs and passive skin samples, we find that:

$$\frac{P_{calcein,LTR}}{P_{calcein,passive}} = \frac{H(\lambda_{calcein})_{LTR}}{H(\lambda_{calcein})_{passive}} \cdot \left[\left(\frac{\varepsilon}{\tau}\right)_{LTR} \Big/ \left(\frac{\varepsilon}{\tau}\right)_{passive}\right] \tag{12}$$

Because the results of the analysis will change slightly based on the chosen frequency (recall the frequency dependence of the pore radius within LTRs, see Table 3), we will consider only the 40 kHz LTR data, since this data lies between the data at 20 kHz and 60 kHz. Similar to the non-LTR analysis presented above, for the LTRs we find that: $\frac{H(\lambda_{calcein})_{LTR}}{H(\lambda_{calcein})_{passive}}=\frac{0.84}{0.020}=42$ and $\left(\frac{\varepsilon}{\tau}\right)_{LTR}/\left(\frac{\varepsilon}{\tau}\right)_{passive}=\frac{1.07\cdot 10^{-3}}{4.17\cdot 10^{-6}}=256$. Using these results in Eq. (12), we clearly see that these two effects account for the observed 4 orders-of-magnitude ($42\times256 = 1.1\cdot 10^{4}$) increase in calcein permeability. For completeness, it is important to stress that either: i) we have underestimated the Δ*x* value used for the LTRs, because the predicted increase in ε/τ (256) is less than the increase expected solely from the 20-fold (276/13.6 = 20, see Table 3) increase in pore radius calculated for the 40-kHz LTRs with respect to native skin ($a_{pore}\sim r_{pore}^{2}=400$), or ii) the number of pores within the LTRs has decreased compared to native skin (this is not unreasonable, since the area of a single pore has increased by 400-fold, and therefore, multiple native skin pores may have merged into a single LTR pore). Note that, with respect to point (i), if a larger Δ*x* value was chosen for the LTR samples than for the passive skin samples, Eq. (12) would need to be modified as follows:

$$\frac{P_{calcein,LTR}}{P_{calcein,passive}}=\underbrace{\frac{H(\lambda_{calcein})_{LTR}}{H(\lambda_{calcein})_{passive}}}_{1}\cdot\underbrace{\frac{\Delta x_{passive}}{\Delta x_{LTR}}}_{2}\cdot\underbrace{\left[\left(\frac{\varepsilon}{\tau}\right)_{LTR}/\left(\frac{\varepsilon}{\tau}\right)_{passive}\right]}_{3} \tag{13}$$

However, as stated previously, this will have no effect on $\frac{P_{calcein,LTR}}{P_{calcein,passive}}$, but simply will cause term 2 in Eq. (13) to decrease linearly with increasing Δx_{LTR}, while term 3 in Eq. (13) will increase linearly with increasing Δx_{LTR} (recall that $\varepsilon/\tau\sim\Delta x$, see Eq. (6)). Therefore, in Eq. (13), the contributions of Δx_{LTR} in terms 2 and 3 will cancel each other. Furthermore, as there is no rigorous method to estimate Δ*x* more accurately, Eq. (13) provides no additional useful information compared to Eq. (12). Also, we note that a similar analysis to that done for the non-LTRs using Eqs. (9) and (10), in order to determine the relative contributions of ε and τ, cannot be carried out for the LTRs because of our uncertainty in the precise value of Δx_{LTR}. In any case, regardless of the value of Δx_{LTR} assumed, the analysis presented here can explain the overall increase in calcein permeability observed within LTRs relative to native skin, since $\frac{P_{calcein,LTR}}{P_{calcein,passive}}$ does not depend on the value of Δx_{LTR} chosen.

Finally, it is important to recognize that the r_{res} values corresponding to the ultrasound frequencies considered here are on the order of tens of microns, while the r_{pore} values calculated in Table 3 are on the order of tens of nanometers. This, however, does not affect our conclusion that transient cavitation collapses near the skin surface are the primary cause for the enlarged pores within LTRs. To reconcile the seemingly large difference between the determined r_{pore} values and the expected r_{res} values at each frequency, we will identify the reasons for this difference in the analysis that follows. First, it is well-known that the r_{res} values represent an upper bound on the average cavitation bubble size in aqueous solution.[49,50] For example, Burdin et al. and Tsochatzidis et al. showed that at 20 kHz, although r_{res} ~ 150 μm, the average bubble radius was calculated to be between 3.15–5.25 μm, depending on the measurement method and the applied ultrasound amplitude, or approximately 25- to 50-fold smaller than the resonant radius.[49,50] In fact, one of the main conclusions of these studies is that the mean measured bubble radius is much smaller than the resonant bubble radius. Second, it has been observed that when transient cavitation bubbles collapse as microjets at an interface, the radius of the impinging microjet is about one order-of-magnitude smaller than the radius of the collapsing cavitation bubble.[45,51] Third, because the skin is an elastic membrane, it is likely to rebound to some extent after a microjet collapses on it. Although there has been no direct research into the actual physical size or shape of the pores left in the skin by collapsing acoustic cavitation microjets, an interesting analogy may be drawn to sharp punctures of the skin by needles and liquid jet injectors. Significant research has been conducted on the penetration of soft solids, such as skin and silicone rubbers, by sharp microscopic objects.[52,53] For example, Shergold *et al.* found, utilizing pig skin and silicone rubbers, that the ratio between the persistent defect left in the skin and the diameter of a sharp tipped object was, in all cases, less than unity (tested for diameters of 300 μm – 2.0 mm), with this ratio ranging between ~0.25–0.6 at the surface of the samples.[53] In addition, Roxhed *et al.* found that a microneedle, with a diameter of 108 μm, left a persistent hole in human skin of only 50 μm, leading these authors to conclude that the persistent damage left in the skin was only about half of the microneedle's shaft diameter.[54] This is relevant to the current analogy because it has recently been shown that liquid jet injectors also penetrate, and damage, the skin in the same manner as sharp-tipped objects puncturing soft materials, such as the skin.[55] Liquid jet injectors transport fluid into the skin by delivering a high-velocity liquid jet (100–200 m/s), having a radius as small as 15 μm, directed at the skin surface,[56] much like an acoustic microjet delivers a liquid jet at the surface of the skin (where the acoustic microjet is expected to have a diameter of ~1 μm or less and have a maximum jet velocity of 153 m/s directed towards the skin[45]). Therefore, the pore radius measured within LTRs are not necessarily equal to the actual radius of the collapsing acoustic microjet itself, but instead, may be equal to the persistent radius of the resulting pore left by the collapsing acoustic microjet. These three mechanisms combined can account for the approximately three orders-of-magnitude difference observed between the expected resonant bubble radii and the calculated r_{pore} values.

Additional research is needed to show definitively that cavitation microjets directed at the skin surface are the primary cause for the formation of pores within LTRs, which would require imaging of the cavitation field above the skin and the pores left within the skin. However, our findings, coupled with the mechanistic analysis described above, provide compelling evidence that this enhancement mechanism is the most likely cause for the observed trend in r_{pore} values seen in the LTRs.

CONCLUSIONS

In this paper, we have shown that the pore radii in the non-LTRs are independent of ultrasound frequency, ranging from 18.2 – 18.5 Å. In addition, we have determined that the pore radii in the non-LTRs are statistically significantly larger than the r_{pore} values for the native skin samples (13.6 Å), suggesting that a frequency-independent enhancement process is at play in these skin regions. Additional experiments were carried out to quantify the amount of SLS penetrating into LTRs and non-LTRs relative to native skin, and we found that nearly twice as much SLS penetrates into the non-LTRs per unit area than into native skin. Furthermore, by studying different mechanisms of SLS penetration into skin, we have shown that boundary-layer reduction caused by microstreaming is the most likely cause for the increased SLS uptake within non-LTRs. Therefore, recognizing that SLS itself can increase pore radii in the skin,[41] we concluded that a frequency-independent process, such as microstreaming, causes increased penetration of SLS into the skin, with SLS acting on the skin being the main contributor to the observed increase in pore radius. In the LTRs, we observed that the pore radii increase dramatically with decreasing frequency (161 Å, 276 Å, and ∞ for 60 kHz, 40 kHz, and 20 kHz LFS, respectively). Accordingly, we have provided strong support to the proposal that transient cavitation events near the skin surface, which are known to be frequency dependent,[10] are the primary mechanism of skin permeability enhancement in LTRs, which is consistent with previous literature findings.[5,6,8,15,21] The variation of the r_{pore} values with ultrasound frequency in the LTRs also suggests that transient cavitation microjets impinging on the skin surface can explain the observed values of the pore radii.

Acknowledgments

We thank Jennifer Seto for her helpful suggestions and significant contribution to the implementation of the theory utilized in this manuscript. We also thank Professor Renata F.V. Lopez and Professor William M. Deen for their useful feedback during the preparation of this manuscript. This research was funded by the National Institute of Health (Grant# EB-00351) and the U.S. Army Research Office through the Institute for Solider Nanotechnologies at MIT (Grant# DAAD-19-02-D-002). PLF acknowledges support from the MIT UROP office. The contents of this manuscript represent solely the views of the authors and do not necessarily reflect the position of the U.S. Government. No official endorsement should be inferred.

References

1. Escobar-Chavez J, Bonilla-Martínez D, Villegas-González M, Rodríguez-Cruz I, Domínguez-Delgado C. The Use of Sonophoresis in the Administration of Drugs Throughout the Skin. J Pharm Pharm Sci 2009;12(1):88. [PubMed: 19470295]
2. Levy D, Kost J, Meshulam Y, Langer R. Effect of ultrasound on transdermal drug delivery to rats and guinea pigs. J Clin Invest 1989;83(6):2074. [PubMed: 2498396]
3. Mitragotri S, Blankschtein D, Langer R. Ultrasound-mediated transdermal protein delivery. Science 1995;269(5225):850–853. [PubMed: 7638603]
4. Johnson ME, Mitragotri S, Patel A, Blankschtein D, Langer R. Synergistic effects of chemical enhancers and therapeutic ultrasound on transdermal drug delivery. J Pharm Sci 1996;85(7):670–679. [PubMed: 8818988]
5. Tezel A, Mitragotri S. Interactions of inertial cavitation bubbles with stratum corneum lipid bilayers during low–frequency sonophoresis. Biophys J 2003;85(6):3502–3512. [PubMed: 14645045]
6. Tezel A, Sens A, Mitragotri S. Investigations of the role of cavitation in low-frequency sonophoresis using acoustic spectroscopy. J Pharm Sci 2002;91(2):444–453. [PubMed: 11835204]
7. Terahara T, Mitragotri S, Langer R. Porous resins as a cavitation enhancer for low-frequency sonophoresis. J Pharm Sci 2002;91(3):753–759. [PubMed: 11920760]
8. Tang H, Wang CC, Blankschtein D, Langer R. An investigation of the role of cavitation in low-frequency ultrasound-mediated transdermal drug transport. Pharm Res 2002;19(8):1160–1169. [PubMed: 12240942]
9. Mitragotri S, Blankschtein D, Langer R. Transdermal drug delivery using low-frequency sonophoresis. Pharm Res 1996;13(3):411–420. [PubMed: 8692734]
10. Gaertner W. Frequency Dependence of Ultrasonic Cavitation. J Acoust Soc Am 1954;26(6):977–980.
11. Khabeev NS. Resonance properties of soluble gas bubbles. Int J Heat Mass Tran 2006;49(5–6):1022–1026.
12. Leighton TG, Walton AJ, Pickworth MJW. Primary Bjerknes forces. Eur J Phys 1990;(1):47.
13. Mitragotri S, Ray D, Farrell J, Tang H, Yu B, Kost J, Blankschtein D, Langer R. Synergistic effect of low-frequency ultrasound and sodium lauryl sulfate on transdermal transport. J Pharm Sci 2000;89(7):892–900. [PubMed: 10861590]
14. Kushner J, Blankschtein D, Langer R. Experimental demonstration of the existence of highly permeable localized transport regions in low-frequency sonophoresis. J Pharm Sci 2004;93(11):2733–2745. [PubMed: 15389675]
15. Tezel A, Sens A, Tuchscherer J, Mitragotri S. Synergistic effect of low-frequency ultrasound and surfactants on skin permeability. J Pharm Sci 2002;91(1):91–100. [PubMed: 11782900]
16. Kushner J, Blankschtein D, Langer R. Evaluation of hydrophilic permeant transport parameters in the localized and non-localized transport regions of skin treated simultaneously with low-frequency ultrasound and sodium lauryl sulfate. J Pharm Sci 2008;97(2):906–918. [PubMed: 17887123]

17. Kushner J, Kim D, So PT, Blankschtein D, Langer RS. Dual-channel two-photon microscopy study of transdermal transport in skin treated with low-frequency ultrasound and a chemical enhancer. J Invest Dermatol 2007;127(12):2832–2846. [PubMed: 17554365]
18. Tezel A, Dokka S, Kelly S, Hardee GE, Mitragotri S. Topical delivery of anti-sense oligonucleotides using low-frequency sonophoresis. Pharm Res 2004;21(12):2219–2225. [PubMed: 15648253]
19. Tezel A, Sens A, Mitragotri S. A theoretical analysis of low-frequency sonophoresis: dependence of transdermal transport pathways on frequency and energy density. Pharm Res 2002;19(12): 1841–1846. [PubMed: 12523663]
20. Tezel A, Sens A, Tuchscherer J, Mitragotri S. Frequency dependence of sonophoresis. Pharm Res 2001;18(12):1694–1700. [PubMed: 11785688]
21. Kushner J, Blankschtein D, Langer R. Heterogeneity in skin treated with low-frequency ultrasound. J Pharm Sci 2008;97(10):4119–4128. [PubMed: 18240305]
22. Tang H, Mitragotri S, Blankschtein D, Langer R. Theoretical description of transdermal transport of hydrophilic permeants: application to low-frequency sonophoresis. J Pharm Sci 2001;90(5): 545–568. [PubMed: 11288100]
23. Kushner J, Blankschtein D, Langer R. Evaluation of the porosity, the tortuosity, and the hindrance factor for the transdermal delivery of hydrophilic permeants in the context of the aqueous pore pathway hypothesis using dual-radiolabeled permeability experiments. J Pharm Sci 2007;96(12): 3263–3282. [PubMed: 17887176]
24. Syracuse Research Corporation. Interactive Physical Properties Database Demo. [Accessed May 18, 2010]. http://www.syrres.com/what-we-do/databaseforms.aspx?id=386
25. Karande P, Jain A, Mitragotri S. Relationships between skin's electrical impedance and permeability in the presence of chemical enhancers. J Control Release 2006;110(2):307–313. [PubMed: 16313994]
26. Tang H, Blankschtein D, Langer R. Effects of low-frequency ultrasound on the transdermal permeation of mannitol: comparative studies with in vivo and in vitro skin. J Pharm Sci 2002;91(8):1776–1794. [PubMed: 12115805]
27. Kasting GB, Bowman LA. Dc Electrical-Properties of Frozen, Excised Human Skin. Pharm Res 1990;7(2):134–143. [PubMed: 2308893]
28. Kasting GB, Bowman LA. Electrical Analysis of Fresh, Excised Human Skin – a Comparison with Frozen Skin. Pharm Res 1990;7(11):1141–1146. [PubMed: 2293212]
29. Rosell J, Colominas J, Riu P, Pallasareny R, Webster JG. Skin Impedance from 1 Hz to 1 Mhz. IEEE T Bio-Med Eng 1988;35(8):649–651.
30. Anderson, R. Clinical Photomedicine. 1993. Optics of the skin; p. 19-35.
31. Anderson R, Parrish J. The optics of human skin. J Invest Dermatol 1981;77(1):13–19. [PubMed: 7252245]
32. Bashkatov A, Genina E, Kochubey V, Tuchin V. Optical properties of human skin, subcutaneous and mucous tissues in the wavelength range from 400 to 2000 nm. J Phys D Appl Phys 2005;38:2543.
33. Jacques S. Origins of tissue optical properties in the UVA, visible, and NIR regions. Advances in Optical Imaging and Photon Migration 1996;2:364–370.
34. Meglinski I, Matcher S. Quantitative assessment of skin layers absorption and skin reflectance spectra simulation. Physiol Meas 2002;23:741–753. [PubMed: 12450273]
35. Dechadilok P, Deen WM. Hindrance factors for diffusion and convection in pores. Ind Eng Chem Res 2006;45(21):6953–6959.
36. Tezel A, Sens A, Mitragotri S. Description of transdermal transport of hydrophilic solutes during low-frequency sonophoresis based on a modified porous pathway model. J Pharm Sci 2003;92(2): 381–393. [PubMed: 12532387]
37. Tezel A, Sens A, Mitragotri S. Incorporation of lipophilic pathways into the porous pathway model for describing skin permeabilization during low-frequency sonophoresis. J Control Release 2002;83(1):183–188. [PubMed: 12220849]
38. Seto J, Polat B, Lopez R, Blankschtein D, Langer R. Effects of ultrasound and sodium lauryl sulfate on the transdermal delivery of hydrophilic permeants: Comparative in vitro studies with

full-thickness and split-thickness pig and human skin. J Control Release. in press. 10.1016/j.jconrel.2010.03.013

39. Edwards DA, Prausnitz MR, Langer R, Weaver JC. Analysis of enhanced transdermal transport by skin electroporation. J Control Release 1995;34(3):211–221.
40. Johnson ME, Blankschtein D, Langer R. Evaluation of solute permeation through the stratum corneum: Lateral bilayer diffusion as the primary transport mechanism. J Pharm Sci 1997;86(10): 1162–1172. [PubMed: 9344175]
41. Ghosh S, Blankschtein D. The role of sodium dodecyl sulfate (SDS) micelles in inducing skin barrier perturbation in the presence of glycerol. Int J Cosmetic Sci 2007;30:73–73.
42. Ghosh S, Blankschtein D. Why is sodium cocoyl isethionate (SCI) mild to the skin barrier? An in vitro investigation based on the relative sizes of the SCI micelles and the skin aqueous pores. J Cosmet Sci 2007;58(3):229–244. [PubMed: 17598025]
43. Moore PN, Puvvada S, Blankschtein D. Challenging the surfactant monomer skin penetration model: Penetration of sodium dodecyl sulfate micelles into the epidermis. 2003;54:29–46.
44. Simonin J-P. On the mechanisms of in vitro and in vivo phonophoresis. J Control Release 1995;33(1):125–141.
45. Fong SW, Klaseboer E, Turangan CK, Khoo BC, Hung KC. Numerical analysis of a gas bubble near bio-materials in an ultrasound field. Ultrasound Med Biol 2006;32(6):925–942. [PubMed: 16785014]
46. Prausnitz MR, Mitragotri S, Langer R. Current status and future potential of transdermal drug delivery. Nat Rev Drug Discov 2004;3(2):115–124. [PubMed: 15040576]
47. Khabeev NS. Resonance Properties of Vapor Bubbles. Pmm-J Appl Math Mec+ 1981;45(4):512–517.
48. Ueda H, Mutoh M, Seki T, Kobayashi D, Morimoto Y. Acoustic Cavitation as an Enhancing Mechanism of Low-Frequency Sonophoresis for Transdermal Drug Delivery. Biol Pharm Bull 2009;32(5):916–920. [PubMed: 19420764]
49. Tsochatzidis NA, Guiraud P, Wilhelm AM, Delmas H. Determination of velocity, size and concentration of ultrasonic cavitation bubbles by the phase-Doppler technique. Chem Eng Sci 2001;56(5):1831–1840.
50. Burdin F, Tsochatzidis NA, Guiraud P, Wilhelm AM, Delmas H. Characterisation of the acoustic cavitation cloud by two laser techniques. Ultrason Sonochem 1999;6(1–2):43–51. [PubMed: 11233937]
51. Kodama T, Tomita Y. Cavitation bubble behavior and bubble-shock wave interaction near a gelatin surface as a study of in vivo bubble dynamics. Appl Phys B-Lasers O 2000;70(1):139–149.
52. Shergold O, Fleck N. Mechanisms of deep penetration of soft solids, with application to the injection and wounding of skin. P Roy Soc Lond A Mat 2004;460(2050):3037.
53. Shergold O, Fleck N. Experimental investigation into the deep penetration of soft solids by sharp and blunt punches, with application to the piercing of skin. J Biomech Eng-T ASME 2005;127:838.
54. Roxhed N, Gasser T, Griss P, Holzapfel G, Stemme G. Penetration-enhanced ultrasharp microneedles and prediction on skin interaction for efficient transdermal drug delivery. J Microelectromech S 2007;16(6):1429.
55. Shergold OA, Fleck NA, King TS. The penetration of a soft solid by a liquid jet, with application to the administration of a needle-free injection. J Biomech 2006;39(14):2593–2602. [PubMed: 16277987]
56. Schramm-Baxter J, Mitragotri S. Needle-free jet injections: dependence of jet penetration and dispersion in the skin on jet power. J Control Release 2004;97(3):527–535. [PubMed: 15212884]

Appendix A – Correcting Sample Absorption Values to Account for Lipid Absorption

A series of twenty negative controls were carried out, identical to the experimental protocol described in the section “Calculating the Steady-State Calcein Permeability,” except that

PBS was used in the donor chamber instead of 0.2% (w/v) calcein in PBS. This was done in order to test if background species, such as skin lipids, could absorb in the receiver solution at the maximum absorbance wavelength for calcein ($\lambda = 494$ nm). We found that there is time-dependent absorbance at a wavelength of 494 nm for the negative controls. However, the level of absorbance was such that it only affected calcein permeability values significantly (>5%) when the total absorbance in the samples containing calcein was below 0.4. Therefore, only the non-LTR samples and the passive control samples were found to be affected significantly by background lipid absorption at 494 nm.

In order to properly account for background lipid absorption in the affected samples, the absorbance intensity as a function of wavelength was measured, in the range 420 nm – 550 nm, for the negative control samples and for samples containing known concentrations of pure calcein. Figure 5 shows the variation of the absorbance with wavelength in: negative control samples containing skin lipids (Figure 5A), samples containing solely calcein (Figure 5B), and non-LTR samples containing a mixture of skin lipids and calcein (Figure 5C). One can clearly see that the curve in Figure 5C is a simple combination of the curves in Figures 5A and 5B.

Unfortunately, the variation in the absorption between samples for the negative controls was too large to simply average the lipid absorption at each sampling time point and then subtract it from the non-LTR and the passive sample data. Fortunately, however, the background absorption for all the negative control samples were found to have similar shapes, indicating that the absorption curve for any of these samples could be reproduced by multiplying a standard background curve (which was generated by averaging the lipid absorption at each wavelength over all the negative control samples) by a constant parameter associated with that given sample. Specifically,

$$\mathrm{A}_i(\lambda)=c_i\mathrm{A}_{sc}(\lambda) \tag{A1}$$

where $\mathrm{A}_i(\lambda)$ is the absorption of sample i at a given wavelength (λ) between 420 – 550 nm, c_i is the constant background parameter associated with that sample, and $\mathrm{A}_{sc}(\lambda)$ is the absorption at a given wavelength for the standard curve.

Therefore, the entire background curve for any sample can simply be defined by a single parameter. In addition, in the negative control samples this parameter is essentially wavelength independent in the relevant range of 420 nm – 550 nm. This indicates that one can extract the background absorbance parameter at any wavelength, or range of wavelengths, and still reconstruct the entire background absorbance curve for the range of wavelengths between 420 nm and 550 nm.

An examination of the plots in Figure 5 shows that in the range 420–430 nm and 540–550 nm there is much larger absorption in the background curve (Figure 5A) than in the pure calcein curve (Figure 5B). As a result, the curve in Figure 5C closely resembles Figure 5A in these two regions. Therefore, in order to decompose a curve like that in Figure 5C into its corresponding background curve (Figure 5A) and pure calcein curve (Figure 5B), the background absorbance parameter was calculated in the range 420–430 nm and 540–550 nm by dividing the absorbance in these regions by the absorbance for that wavelength in the standard background curve. Subsequently, the simple arithmetic mean of these twenty-two values was calculated to obtain the background absorbance parameter for that sample, and the background curve was reconstructed by multiplying the calculated parameter by the standard background curve. The calculated background curve (such as Figure 5A) was then subtracted from the total curve (such as Figure 5C) in order to construct a pure calcein curve (such as Figure 5B) for that sample. The resulting curve was then used to calculate the concentration of calcein in the receiver chamber.

In order to validate that the decomposition method described above yields reproducible and reliable calcein concentrations, a series of 10 samples with predetermined absorption profiles of background lipids and predetermined absorption profiles of pure calcein were mixed. The actual concentration of calcein was compared to the value obtained using our decomposition method, and the difference between the calcein concentration calculated by the decomposition method and the actual calcein concentration in each case was found to be less than ~5%, thereby validating this method.

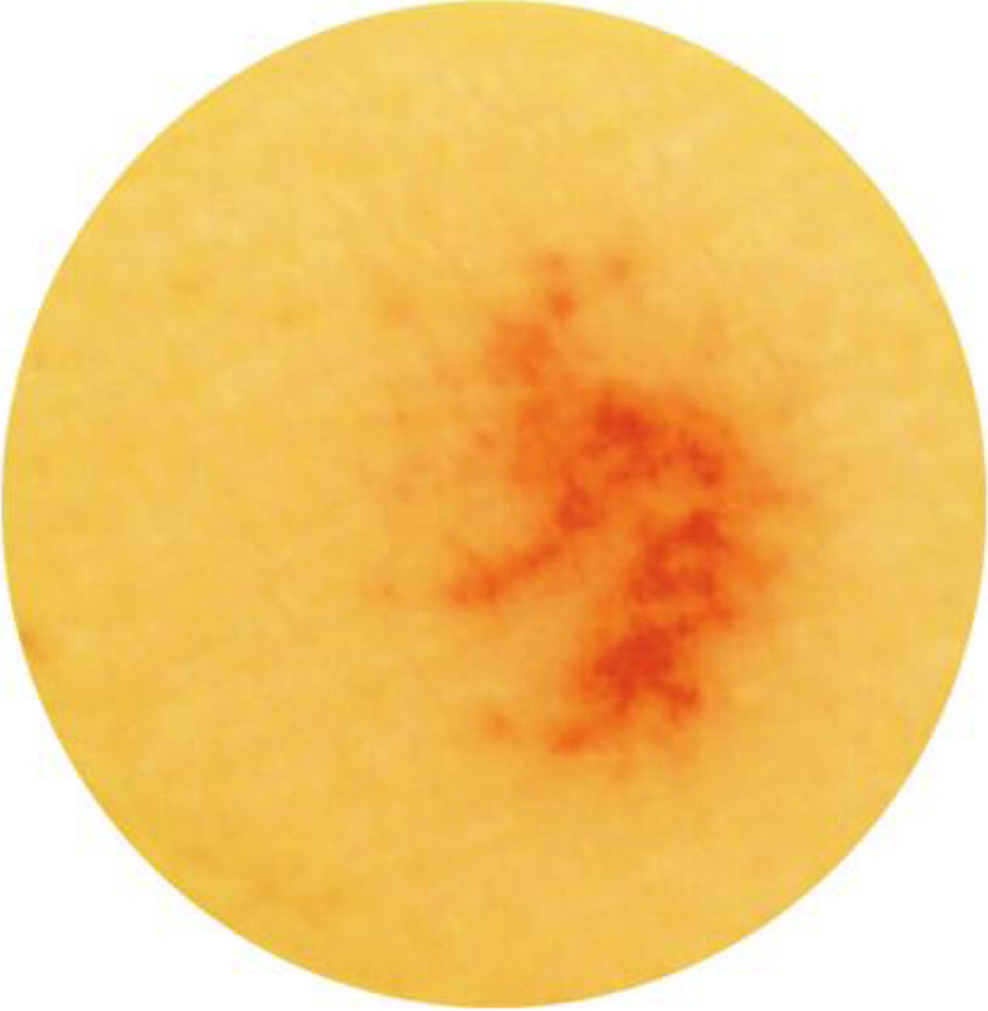

Figure 1.

Porcine skin sample treated with LFS/SLS at 40 kHz. Regions of the skin dyed red are LTRs, regions of the skin that are not dyed red are non-LTRs. The diameter of the circular sample is 15 mm.

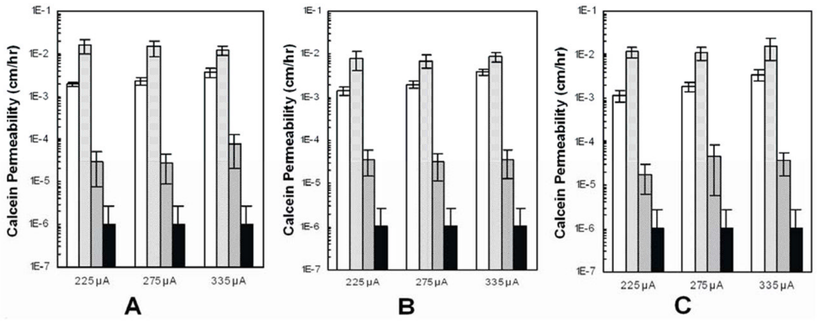

Figure 2.

Calcein Permeability for the total, LTR, non-LTR, and passive skin samples treated to electrical current thresholds of 225 μA, 275 μA, and 335 μA at the three ultrasound frequencies considered: 20 kHz (A), 40 kHz (B), and 60 kHz (C). Key: Total group (□); LTR group(▦); Non-LTR group (▧); Passive group (■). Error bars = ±1 SD. Each bar in each graph represents 8–12 samples, except for the passive group where the sample size is 20.

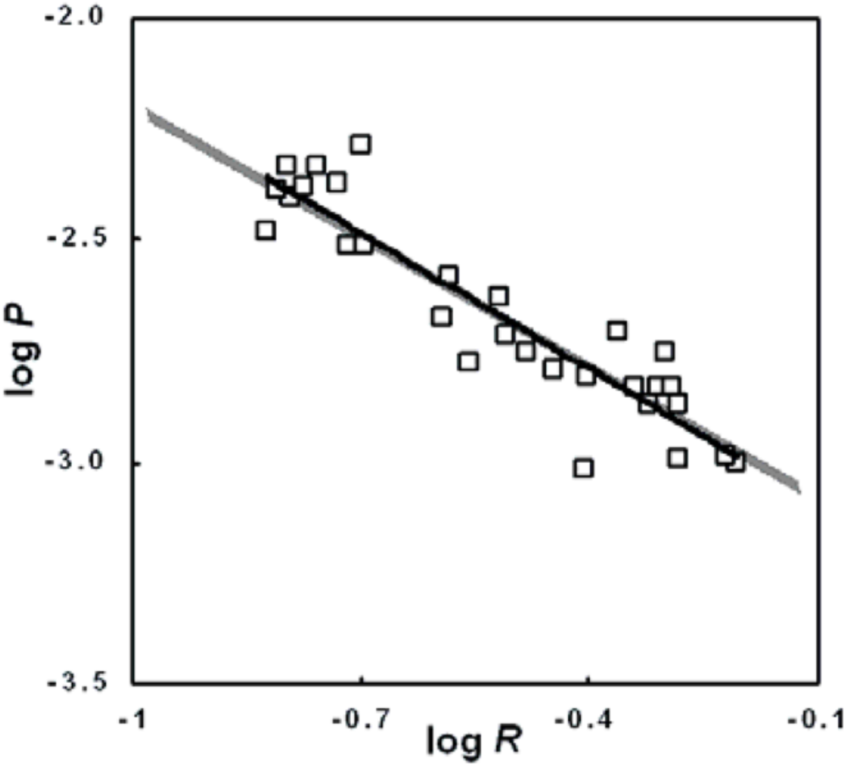

Figure 3.

Sample log *P* vs. log *R* plot. Data shown (□) is for LTR samples treated at 40 kHz. Units of *P* are cm/hr and units of *R* are kOhm·cm^2. Key: solid black line – linear regression of the data, gray line – linear regression with theoretical slope of −1.

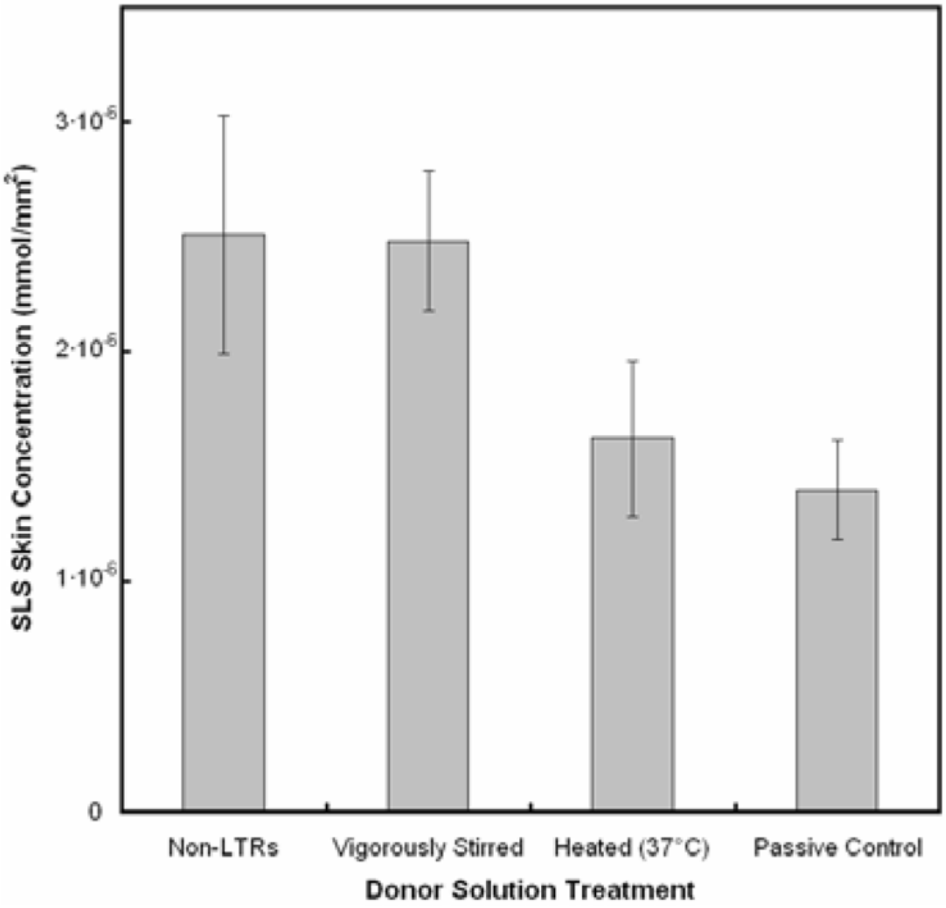

Figure 4.

Concentration of SLS in skin treated under different experimental conditions in the donor solution, compared to that of non-LTRs. In each case, the total concentration of SLS in the donor solution was 1% (w/v), but stirring and heating (37° C) were varied in order to assess the importance of these two processes on SLS penetration within non-LTRs. Error bars shown are 95% confidence intervals.

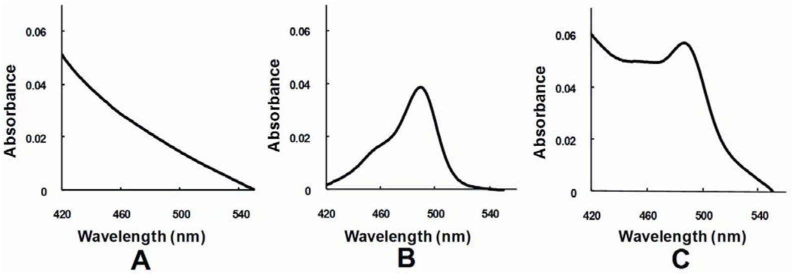

Figure 5.
Absorption as a function of wavelength, in the range 420 – 550 nm, for: a background sample containing skin lipids (A), a pure calcein sample (B), and a non-LTR sample containing both calcein and skin lipids (C).

Table 1

LTR area as a function of skin electrical current threshold and ultrasound frequency. The total skin area of the samples is 1.77 cm^2.

	20 kHz		40 kHz		60 kHz	
Current Threshold	**n**	**LTR Area (cm^2) [a]**	**n**	**LTR Area (cm^2) [a]**	**n**	**LTR Area (cm^2) [a]**
225	18	0.197±0.070	16	0.282±0.079	15	0.154±0.034
275	17	0.265±0.055	19	0.399±0.080	19	0.327±0.102
335	17	0.531±0.099	20	0.452±0.066	21	0.417±0.117

[a] Range corresponds to a 95% confidence interval.

Table 2

Statistical analysis on the slopes of log *P* as a function of log *R* for all the data sets tested. The 95% confidence interval for the slope must contain the value −1 for the aqueous porous pathway model to be applicable.

	Total			LTRs			Non-LTRs		
Frequency	**n**	**Slope** [a]	r^2	**n**	**Slope** [a]	r^2	**n**	**Slope** [a]	r^2
20 kHz	35	−0.92 ± 0.17	0.79	28	−1.01±0.26	0.71	24	−1.24±0.38	0.68
40 kHz	30	−1.02 ± 0.16	0.85	27	−1.02±0.26	0.73	30	−1.13±0.22	0.79
60 kHz	36	−1.08 ± 0.21	0.76	30	−0.95±0.32	0.57	30	−1.07±0.27	0.70
Passive	20	−1.14 ± 0.73	0.16						

[a] Range corresponds to a 95% confidence interval.

Table 3

Pore radii calculated for the total, LTR, non-LTR, and passive skin samples, as a function of the ultrasound frequency. The lower and upper bounds correspond to the endpoints of the 95% confidence interval of the pore radius.

	Total			**LTRs**			**Non-LTRs**		
Frequency	**Lower**	**r_{pore}(Å)**	**Upper**	**Lower**	**r_{pore}(Å)**	**Upper**	**Lower**	**r_{pore}(Å)**	**Upper**
20 kHz	81.5	105	148	-----	-----	-----	17.0	18.5	20.4
40 kHz	61.6	73.9	92.9	165	276	-----	17.2	18.2	19.4
60 kHz	43.6	50.7	61.1	97.2	161	-----	17.3	18.4	19.8
Passive	12.9	13.6	14.4						